inorganics

MDPI

Article

Synthesis and Characterization of New Copper(II) Coordination Compounds with Methylammonium Cations

Amalija Golobič [1], Brina Dojer [2], Marko Jagodič [3], Anja Siher [4], Anže Pegan [5] and Matjaž Kristl [5,*]

[1] Faculty of Chemistry and Chemical Technology, University of Ljubljana, Večna Pot 113, SI-1000 Ljubljana, Slovenia; amalija.golobic@fkkt.uni-lj.si
[2] Faculty of Natural Sciences and Mathematics, University of Maribor, Koroška cesta 160, SI-2000 Maribor, Slovenia; brina.dojer@um.si
[3] Institute of Mathematics, Physics and Mechanics, Jadranska 19, SI-1000 Ljubljana, Slovenia; marko.jagodic@imfm.si
[4] Materials Research Laboratory, University of Nova Gorica, Vipavska 11c, SI-5270 Ajdovščina, Slovenia; anja.siher@ung.si
[5] Faculty of Chemistry and Chemical Engineering, University of Maribor, Smetanova 17, SI-2000 Maribor, Slovenia; anze.pegan@student.um.si
* Correspondence: matjaz.kristl@um.si

Abstract: We synthesized four new copper(II) complexes with acetato and chlorido ligands and methylammonium (MA), dimethylammonium (DMA), and tetramethylammonium (TMA) counterions: $(MA)_4[Cu_2Ac_4Cl_2]Cl_2{\cdot}2H_2O$ (**1**), $(DMA)_2[Cu_2Ac_4Cl_2]$ (**2**), $(DMA)_4[Cu_2Ac_4Cl_2]Cl_2{\cdot}2H_2O$ (**3**), and $(TMA)_5[Cu_2Ac_4Cl]Cl_4{\cdot}4H_2O$ (**4**). All compounds were characterized by single-crystal X-ray diffraction, magnetic measurements, FTIR spectroscopy, and thermogravimetric analysis. Complexes **1**, **2**, and **3** consist of a dinuclear coordination anion $[Cu_2(Ac)_4Cl_2]^{2-}$ with bridging acetato ligands arranged in a paddle-wheel conformation and square-pyramidal coordination around Cu(II) atoms, while the coordination anion in compound **4** is a polymeric chain, parallel to the ***c*** axis, with $Cu_2(Ac)_4$ units connected through bridging chlorido ligands. Magnetic measurements carried out between 2 K and 300 K indicate strong antiferromagnetic interactions between Cu(II) ions. The effective magnetic moments range from 1.94 μ_B to 2.21 μ_B, exceeding the spin-only value for Cu(II) ions ($\mu_{eff} = 1.73\ \mu_B$) and suggesting significant orbital contributions to the magnetic moment. Thermogravimetric analysis of all complexes showed a multistep decomposition behavior yielding elemental copper as the final product.

Keywords: copper(II) coordination compounds; methylamines; crystal structure; magnetic properties; thermogravimetric analysis

check for updates

Citation: Golobič, A.; Dojer, B.; Jagodič, M.; Siher, A.; Pegan, A.; Kristl, M. Synthesis and Characterization of New Copper(II) Coordination Compounds with Methylammonium Cations. *Inorganics* **2024**, *12*, 261. https://doi.org/10.3390/inorganics12100261

Academic Editors: Wolfgang Linert and Steve Liddle

Received: 29 August 2024
Revised: 25 September 2024
Accepted: 26 September 2024
Published: 29 September 2024

Copyright: © 2024 by the authors. Licensee MDPI, Basel, Switzerland. This article is an open access article distributed under the terms and conditions of the Creative Commons Attribution (CC BY) license (https://creativecommons.org/licenses/by/4.0/).

1. Introduction

Recent years have seen an increased interest in the preparation and investigation of organic–inorganic hybrid perovskites with the general formula ABX_n, where A is a small organic cation, B is a divalent cation, and X is a halogen. The most commonly investigated among this class of materials is methylammonium (MA) lead iodide, which is one of the most promising photovoltaic materials with power conversion efficiency higher than 20% [1–4]. However, due to concerns about lead toxicity, organic–inorganic tin(II) halide perovskites with the general formula $MSnX_3$ (X = Cl, Br) have emerged as promising alternatives [5], where A is typically a small cation such as MA. Other examples of methylammonium metal halides are $(MA)AgBr_2$ and $(MA)Ag_2I_3$, showing potential as wide band-gap semiconductors with good thermal stability [6]. Gold perovskites with the formula $M_2[Au^{I}I_2][Au^{III}I_4]$, where M is small organic cations like MA or dimethylammonium (DMA), have recently also been reported to be promising candidates for solar cell materials, showing that the optical band gap increased as the size of the cation became

larger [7]. Syntheses and structures of MA cobalt formate, $MA[Co(HCOO)_3]$, MA zirconium fluoride, $MA[ZrF_5]\cdot 0.5H_2O$, and chloroantimonates with DMA cations, with the formula $(DMA)_3[Sb_2Cl_9]$, have also been reported [8–10].

While copper coordination compounds have been intensively studied over decades due to their structural variety and extensive practical usage, including catalysts, fungicides/pesticides, pigments, and high-temperature superconductors [11], the research of copper complexes with MA and DMA cations seems to be limited. Structures of $(MA)_2[Cu(NO_3)_4]$ and Cu(II) complexes with MA cations and 1-hydroxyethane-1,1-diphosphonato ligands have been reported [12,13], as well as those of Cu(I) coordination frameworks with MA and chloride [14]. Photochromic behavior in $(MA)_2CuCl_4$ has been investigated recently [15].

Among copper(II) complexes with DMA cations, structures of compounds comprising pyridine-2,5-dicarboxylatoand pyrazole-3,5-dicarboxylato ligands, and three different compounds with sulfato ligands have been reported [16–18]. Structures and properties of copper(II) coordination compounds with chlorate ligands and DMA cations have also been reported [19,20], exhibiting appealing magnetic and ferroelectric properties. Crystal structures and magnetic behavior of mixed cation salts (DMA)(3,5-dimethylpyridinium)CuX_4, X = Cl, Br have also been investigated [21]. Research of Cu(II) coordination polymer with DMA cation and pyridine-2,5-dicarboxylic acid ligand revealed a substantial inhibitory activity against both Gram-positive and -negative bacteria [22]. Coordination compounds of other transition metals containing DMA cations, most often those with an Fe(III) central ion, are under investigation in the development of advanced functional materials, e.g., in photovoltaic cells and drug delivery systems [23], as spin-crossover magnetic materials [24] and as antibacterial agents [25]. Zinc complexes with DMA are a research focus due to their unusual electrical properties [26], while rare-earth complexes containing DMA cations and pyridine-2,6-dicarboxylic acid ligands have attracted attention as fluorescence materials [27,28].

Among reported copper coordination compounds with tetramethylammonium (TMA) cation and various ligands, a variety of structures can be revealed. The structure of $(TMA)[Cu(N_3)_3]$ consists of chains formed by copper(II) ions bridged by end-to-end and end-on azido ions in a honeycomb-like arrangement [29], while mixed halogeno(cyano)cuprates, $(TMA)[Cu_3(CN)_2Br_2]$ and $(TMA)_2[Cu_4(CN)_5Cl]$ form 1D–ribbonlike chains and 3D nanoporous frameworks [30]. Structural investigations of a series of copper complexes with iodato ligands and tetraalkylammonium cations NR_4^+, the smallest one being TMA, revealed how the structure of the products depends on the size of the counterion, with smaller ions like TMA tending to produce chain-like structures, while for larger tetraalkylammonium species, complex $[Cu_xI_y]$ clusters were observed [31]. The structure of a similar complex with the oxalate ligand, $(TMA)_2[Cu(C_2O_4)_2]\cdot H_2O$, consists of anionic oxalate-bridged copper(II) chains, TMA cations, and uncoordinated water molecules, with oxalate ligands being in bidentate and bis-bidentate bridging mode [32]. Two copper(II) complexes with the ligand *N*,*N*′-2,6-pyridinebis(oxamic acid), mpyba, were reported [33], consisting of $^-$metallamacrocycle entities with five-coordinate copper and TMA counterions. Using the ligand (*S*)-*N*-(ethyl oxoacetate)alanine, a rod-like metal organic framework (MOF) was synthesized, featuring an interesting structure consisting of anionic cyclic hexacopper 'wheels' templated by TMA cations [34]. Three TMA cyanocuprates(I), forming 3D networks of copper ions, crosslinked by cyano ligands, with TMA ions lying in the as-formed channels, have been reported [35]. Investigation of optical properties of these materials revealed optical memory behavior, with the ability to undergo a reversible change in emission upon laser irradiation. Recently, a novel perovskite-like complex with the formula $(TMA)Cu_2Br_3$ was investigated [36], featuring an impressive photovoltaic effect due to the emergence of excitonic Cu(I)–Cu(I) interactions.

The main purpose of this work was to investigate new coordination compounds of copper(II) with acetate and chloride ligands and different methylammonium cations and grow crystals suitable for structural determination. Four new compounds with MA, DMA,

and TMA cations were obtained and structurally identified. The thermal behavior of all compounds was investigated, and their magnetic properties are reported.

2. Experimental Setup

All starting compounds and solvents were used without further purification and purchased from commercial sources as follows: methylammonium chloride (CH_3NH_3Cl, 99%) and dimethylammonium chloride ($(CH_3)_2NH_2Cl$, 99%) were purchased from Acros Organics. Tetramethylammonium fluoride tetrahydrate ($(CH_3)_4NF{\cdot}4H_2O$, 98%) and copper(II) acetate monohydrate (>99.0%) were obtained from Merck. The solvents methanol (≥99.8%) and acetonitrile (99.8%) were obtained from Sigma-Aldrich (St. Louis, MO, USA), while absolute ethanol (≥99.9%) was purchased from Carlo Erba Reagents. Elemental analysis was carried out using a Perkin Elmer CHNS/O 2400 Series II elemental analyzer (PerkinElmer, Inc., Waltham, MA, USA) at the Faculty of Chemistry and Chemical Engineering in Maribor. The content of copper was measured on a Varian SpectrAA-10 flame atomic spectrometer (AAS; Varian, Palo Alto, CA, USA).

2.1. Synthesis of $(MeNH_3)_4[Cu_2Ac_4Cl_2]Cl_2{\cdot}2H_2O$ (1)

For the synthesis of **1**, we dissolved 0.0684 g (=1.01 mmol) of methylammonium chloride in 20 mL of methanol and added 0.2014 g (=1.01 mmol) of copper(II) acetate monohydrate under constant stirring by a magnetic stirrer. The solution was stirred for a further 90 min and allowed to stand at room temperature (RT) for several days. Light-blue and dark-blue crystals formed in the mother liquor. The light-blue product turned out to be the new complex **1**, while the dark-blue crystals were identified as tetrakis(μ_2-acetato)-diaqua-di-copper(II) [37]. The co-crystallized materials were manually separated. It is worthwhile to mention that a mixture of identical products, e.g., **1** and tetrakis(μ_2-acetato)-diaqua-di-copper(II), was also obtained when using ethanol as a solvent. Anal. calc. for $C_{12}H_{40}Cl_4Cu_2N_4O_{10}$ (M_r = 669.38): C, 21.53%; H, 6.02%; Cl, 21.19%; Cu, 18.99%; N, 8.37%; O, 23.90%. Found: C, 21.35%; H, 6.14%; Cu, 19.14%; N, 8.28%; O, 23.42%.

2.2. Synthesis of $(NH_2Me_2)_2[Cu_2Ac_4Cl_2]$ (2)

During the preparation of **2**, we dissolved 0.0808 g (=0.997 mmol) of dimethylammonium chloride in 20 mL of ethanol and added 0.1997 g (=1.00 mmol) of copper(II) acetate monohydrate under constant stirring. After stirring for 90 min, the solution was allowed to stand at RT for several days. Light-blue and dark-blue crystals formed in the mother liquor. The light-blue product turned out to be the new complex **2**, while the dark-blue crystals were identified as tetrakis(μ_2-acetato)-diaqua-di-copper(II) [37]. The co-crystallized materials were manually separated. Anal. calc. for $C_{12}H_{28}Cl_2Cu_2N_2O_8$ (M_r = 526.36): C, 27.38%; H, 5.36%; Cl, 13.47%; Cu, 24.15%; N, 5.32%; O, 24.32%. Found: C, 27.22%; H, 5.22%; Cu, 24.22%; N, 5.27%; O, 24.41%.

2.3. Synthesis of $(NH_2Me_2)_4[Cu_2Ac_4Cl_2]Cl_2{\cdot}2H_2O$ (3)

For the synthesis of **3**, we dissolved 0.1613 g (=1.978 mmol) of dimethylammonium chloride and 0.1803 g (=0.903 mmol) of copper(II) acetate monohydrate in 20 mL of methanol using magnetic stirring. The solution was stirred for another 90 min and subsequently allowed to stand at RT for several days. Cyan crystals formed in the mother liquor, which were identified as the new complex **3**. Anal. calc. for $C_{16}H_{48}Cl_4Cu_2N_4O_{10}$ (M_r = 725.46): C, 26.49%; H, 6.67%; Cl, 19.55%; Cu, 17.52%; N, 7.72%; O, 22.05%. Found: C, 26.61%; H, 6.68%; Cu, 17.41%; N, 7.81%; O, 22.11%.

2.4. Synthesis of $(NMe_4)_{5n}[Cu_2Ac_4Cl]_nCl_{4n}{\cdot}4nH_2O$ (4)

To obtain complex **4**, we dissolved 0.1586 g (=0.960 mmol) of tetramethylammonium fluoride tetrahydrate in 20 mL of acetonitrile. Under constant stirring, 0.0786 g (=0.964 mmol) of dimethylammonium chloride and 0.1907 g (=0.955 mmol) of copper(II) acetate monohydrate were added. The solution was stirred for a further 90 min and allowed

to stand at RT. Light-blue crystals, which were later identified to be the new complex **4**, formed in the mother liquor after one day. Anal. calc. for $C_{28}H_{80}Cl_5Cu_2N_5O_{12}$ (M_r = 983.32): C, 34.20%; H, 8.20%; Cl, 18.03%; Cu, 12.92%; N, 7.12%; O, 19.53%. Found: C, 34.11%; H, 8.16%; Cu, 12.77%; N, 7.11%; O, 19.62%.

2.5. X-ray Crystallography

Single-crystal diffraction data of compounds **1–4** were collected using MoKα radiation and ω scans at 150(1) K on an Agilent SuperNova dual-source diffractometer with an Atlas detector and mirror monochromator. The data were processed using CrysAlis PRO 1.171.39.46e [38], with multi-scan empirical absorption correction. Structures were solved by direct methods using SIR97 [39]. A full-matrix, least-squares refinement of F^2 was employed with anisotropic temperature-displacement parameters for the non-hydrogen atoms. H atoms in all structures were observed in difference Fourier maps. Nevertheless, H atoms from methyl groups were treated as riding with an HFIX option of 137. H atoms bonded to nitrogen and oxygen atoms were located from difference Fourier maps. Their positions were refined together with an isotropic displacement parameter. In compounds **1** and **4**, restraints on O-H distances in water molecules were applied. SHELXL-2018/3 software [40] was used for structure refinement and interpretation. Drawings of the structures were produced using ORTEPIII [41] and Mercury [42]. Details of crystal data, data collection, and structure refinement are given in Table 1. All crystallographic details for structures of **3**, **4**, **1**, and **2** have also been deposited with the Cambridge Crystallographic Data Centre as deposition numbers 2379668–2379671, respectively. These data can be obtained free of charge via www.ccdc.cam.ac.uk/conts/retrieving.html (or from the CCDC, 12 Union Road, Cambridge CB2 1EZ, UK; fax: +44 1223 336033; e-mail: deposit@ccdc.cam.ac.uk).

Table 1. Experimental data for the X-ray diffraction studies of compounds **1–4**.

	1	**2**	**3**	**4**
Formula	$C_{12}H_{40}Cl_4Cu_2N_4O_{10}$	$C_{12}H_{28}Cl_2Cu_2N_2O_8$	$C_{16}H_{48}Cl_4Cu_2N_4O_{10}$	$C_{28}H_{80}Cl_5Cu_2N_5O_{12}$
M_r	669.38	526.36	725.46	983.32
crystal system	monoclinic	monoclinic	triclinic	tetragonal
space group	$P2_1/c$, no.14	$P2_1/n$, no.14	P-1, no.2	I-4, no.82
a (Å)	11.9035(10)	7.8045(4)	9.0370(6)	17.4217(4)
b (Å)	8.9511(7)	11.9619(8)	9.2174(6)	17.4217(4)
c (Å)	14.6769(14)	11.0067(6)	11.8008(7)	7.8915(3)
α (°)	90.00	90.00	99.455(5)	90
β (°)	112.971(11)	95.143(5)	102.404(5)	90
γ (°)	90.00	90.00	115.525(6)	90
V (Å^3)	1439.8(2)	1023.41(10)	828.73(10)	2395.19(14)
Z	2	2	1	2
calc. density (g cm^{-3})	1.544	1.708	1.454	1.363
MoKα radiation (Å)	0.71073	0.71073	0.71073	0.71073
μ (mm^{-1})	1.894	2.378	1.652	1.220
crystal color and form	blue prism	blue prism	blue prism	blue prism
crystal dimensions	0.15 × 0.15 × 0.40	0.12 × 0.23 × 0.27	0.25 × 0.35 × 0.35	0.07 × 0.07 × 0.16
reflections measured	7384	5517	7807	25,010
θ range (°)	2.7–30.2	3.5–29.9	2.6–30.3	2.8–30.3
h, k, l range measured	−15→15; −12→12; −19→19	−11→7; −10→16; −12→14	−11→12; −12→11; −16→15	−23→24; −23→24; −11→10
no. of independent refl.	3740	2705	4291	3454
R_{int}	0.027	0.035	0.025	0.037
observed r., $F^2 > 2\sigma(F^2)$	3001	2324	3481	3196
R[$F^2 > 2\sigma(F^2)$]	0.030	0.030	0.033	0.023
$wR(F^2)$, all data	0.072	0.072	0.083	0.057
goodness-of-fit, S	0.990	1.062	1.068	1.081
no. of contrib. reflect.	3740	2705	4291	3454
no. of parameters	181	130	193	133
$\Delta\rho_{max}$, $\Delta\rho_{min}$ (eÅ^{-3})	0.469, −0.512	0.453, −0.566	0.636, −0.540	0.283, −0.268

2.6. IR Spectroscopy

Infrared spectra were taken on a Perkin Elmer FTIR spectrometer (PerkinElmer, Inc., Waltham, MA, USA) at room temperature on solid samples, using ATR in the range 650–4000 cm^{-1}.

2.7. Magnetic Measurements

The temperature dependence of magnetic susceptibility $\chi(T)$ for samples **1**–**4** was measured between 2 K and 300 K in a DC magnetic field of 1000 Oe using a Quantum Design MPMS XL-5 magnetometer (Quantum Design, San Diego, CA, USA). The data were corrected for the contribution of the sample holder and temperature-independent diamagnetism of inner-shell electrons using Pascal's tables [43].

2.8. Thermal Analysis and X-ray Powder Diffraction

The thermal decomposition of compounds **1**–**4** was studied on a Mettler TGA 2 system (Mettler-Toledo, Columbus, OH, USA) in the temperature range 30–900 °C, using 70 µL Al_2O_3 crucibles, a heating range of 10 °C/min, and nitrogen flow atmosphere (50 mL/min). The final products of the decomposition were characterized with an AXS-Bruker/Siemens D5005 diffractometer (Bruker, Billerica, MA, USA), utilizing graphite monochromated CuK_α radiation (λ = 1.54178 Å) and a silicon single-crystal holder.

3. Results and Discussion

3.1. Description of Structures

Crystal structures of compound **1** with the formula $(MeNH_3)_4[Cu_2Ac_4Cl_2]Cl_2{\cdot}2H_2O$, compound **2** with the formula $(NH_2Me_2)_2[Cu_2Ac_4Cl_2]$, compound **3** with the formula $(NH_2Me_2)_4[Cu_2Ac_4Cl_2]Cl_2{\cdot}2H_2O$, and compound **4** with the formula $(NMe_4)_{5n}[Cu_2Ac_4Cl]_nCl_{4n}{\cdot}4nH_2O$ are presented in Figures 1–4, respectively. Selected bond lengths in compounds **1**–**4** are given in Table 2.

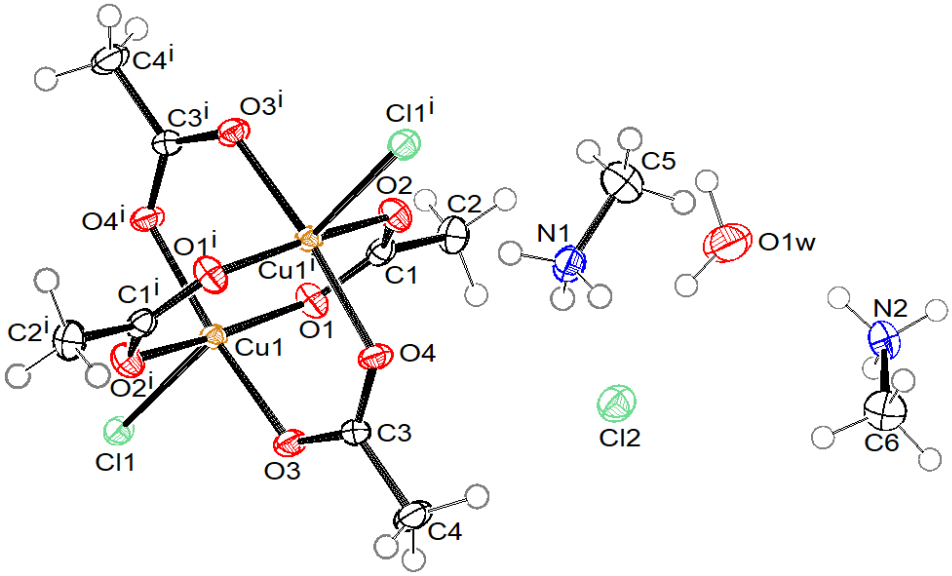


Figure 1. ORTEP drawing of compound **1** with labelling of non-H atoms. Ellipsoids are drawn at 50% level. (*i:* $-x + 1, -y, -z + 1$.)

Compounds **1**, **2**, and **3** consist of a centrosymmetric dinuclear coordination anion $[Cu_2(Ac)_4Cl_2]^{2-}$ with the paddle-wheel conformation, where Cu(II) atoms have a square-pyramidal coordination. The basal plane is formed by four O atoms of four bridging acetate ions at bond distances in the range of 1.9553(13) and 1.9825(14) Å. The terminal apical chlorido ligand is bonded at distance 2.4610(5), 2.4626(6), and 2.4569(6) Å in **1**, **2**, and **3**, respectively. In compounds **1** and **3**, the asymmetric unit consists of half of a complex anion,

one uncoordinated chloride anion, one water molecule, and two cations (methyammonium in **1** and dimethylammonium in **3**). In compound **2**, the asymmetric unit contains half of the complex anion and a dimethylammonium cation only.

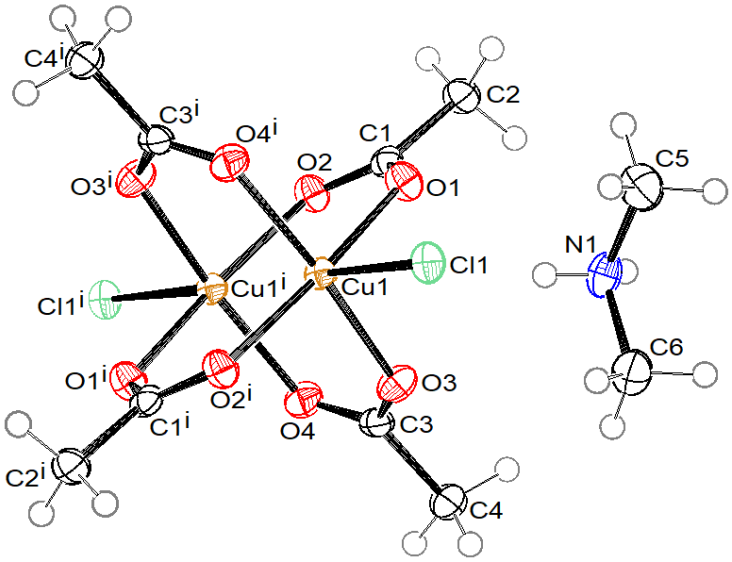


Figure 2. ORTEP drawing of compound **2** with labelling of non-H atoms. Ellipsoids are drawn at 50% level. (*i:* $-x + 1, -y, -z + 1$.)

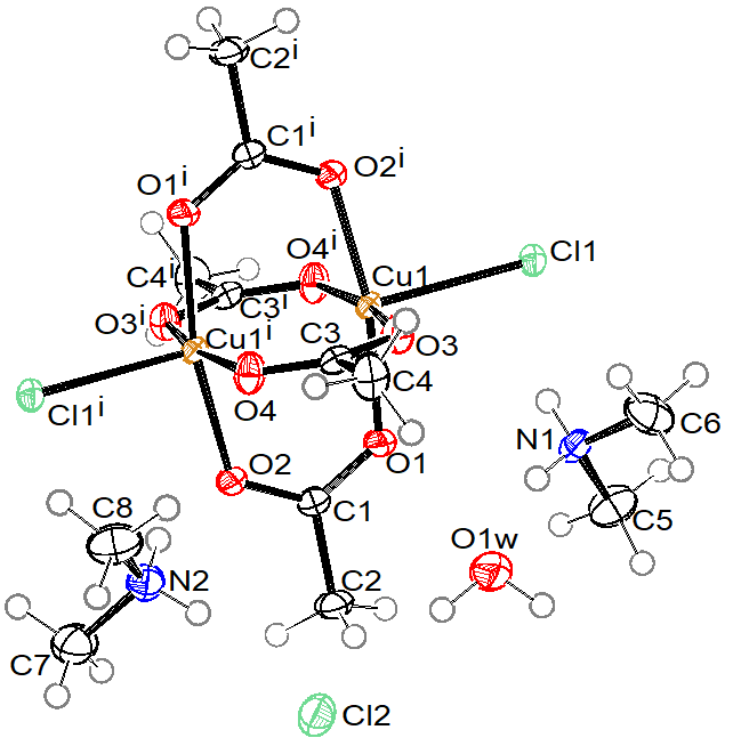


Figure 3. ORTEP drawing of compound **3** with labelling of non-H atoms. Ellipsoids are drawn at 50% level. (*i:* $-x + 1, -y, -z + 1$.)

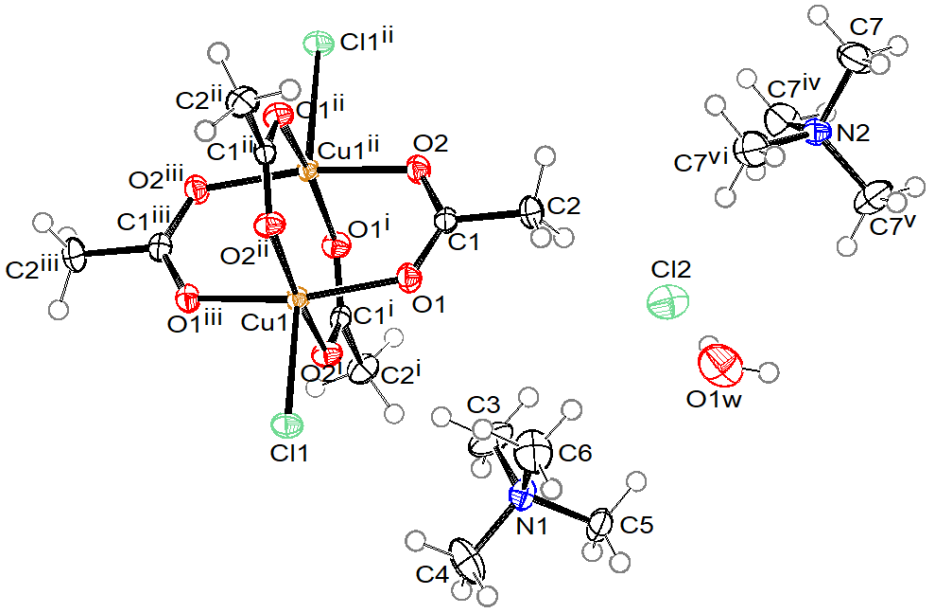


Figure 4. ORTEP drawing of compound **4** with labelling of non-H atoms. Ellipsoids are drawn at 50% level. (*i:* $-y + 1/2, x + 1/2, -z + 3/2$; *ii:* $y-1/2, -x + 1/2, -z + 3/2$; *iii:* $-x, -y + 1, z$; *iv:* $1 - x, 1 - y, z$; *v:* $1 - y, x, 2 - z$; *vi:* $y, 1 - x, 2 - z$.)

Table 2. Selected bond lengths (Å) and angles (°) for compounds **1**–**4**.

1			
Cu1—O1	1.9554 (13)	O4^{i}—Cu1—O3	168.91 (6)
Cu1—O4^{i}	1.9685 (13)	O4^{i}—Cu1—O2^{i}	87.24 (6)
Cu1—O3	1.9719 (13)	O3—Cu1—O2^{i}	89.41 (6)
Cu1—O2^{i}	1.9789 (13)	O1—Cu1—Cl1	98.60 (4)
Cu1—Cl1	2.4610 (5)	O4^{i}—Cu1—Cl1	96.78 (4)
Cu1—Cu1^{i}	2.6033 (5)	O1—Cu1—O2^{i}	169.31 (6)
O1—Cu1—O4^{i}	91.85 (6)	O3—Cu1—Cl1	93.90 (5)
O1—Cu1—O3	89.49 (6)	O2^{i}—Cu1—Cl1	92.08 (4)
(i) $-x + 1, -y, -z + 1$			
2			
Cu1—O4^{i}	1.9707 (14)	O4^{i}—Cu1—O3	167.36 (7)
Cu1—O3	1.9731 (14)	O4^{i}—Cu1—O1	90.68 (6)
Cu1—O1	1.9800 (14)	O3—Cu1—O1	86.63 (6)
Cu1—O2^{i}	1.9825 (14)	O4^{i}—Cu1—O2^{i}	88.60 (6)
Cu1—Cl1	2.4626 (6)	O3—Cu1—O2^{i}	91.33 (6)
Cu1—Cu1^{i}	2.6706 (5)	O1—Cu1—O2^{i}	167.30 (6)
O1—Cu1—Cl1	95.28 (5)	O4^{i}—Cu1—Cl1	96.97 (5)
O2^{i}—Cu1—Cl1	97.39 (5)	O3—Cu1—Cl1	95.57 (5)
(i) $-x + 1, -y, -z + 1$			
3			
Cu1—O4^{i}	1.9663 (14)	O4^{i}—Cu1—O3	168.30 (6)
Cu1—O3	1.9671 (14)	O4^{i}—Cu1—O1	90.47 (6)
Cu1—O1	1.9711 (14)	O3—Cu1—O1	88.81 (6)
Cu1—O2^{i}	1.9783 (14)	O4^{i}—Cu1—O2^{i}	87.93 (6)
Cu1—Cl1	2.4569 (6)	O3—Cu1—O2^{i}	90.40 (6)
Cu1—Cu1^{i}	2.6390 (5)	O1—Cu1—O2^{i}	168.22 (6)
O1—Cu1—Cl1	97.73 (5)	O4^{i}—Cu1—Cl1	96.49 (5)
O2^{i}—Cu1—Cl1	94.04 (5)	O3—Cu1—Cl1	95.17 (5)
(i) $-x + 1, -y, -z + 1$			
4			
Cu1—O2^{i}	1.9647 (15)	O2^{i}—Cu1—O2^{ii}	168.37 (9)
Cu1—O1^{iii}	1.9673 (15)	O2^{ii}—Cu1—O1	89.13 (8)
Cu1—Cl1	2.6094 (3)	O2^{i}—Cu1—Cl1	95.81 (4)
Cu1—Cu1^{ii}	2.6726 (6)	O2^{i}—Cu1—O1	89.53 (8)
O1—Cu1—Cl1	96.62 (4)	O1^{iii}—Cu1—O1	166.77 (9)
(i) $-y + 1/2, x + 1/2, -z + 3/2$;	*(iii)* $-x, -y + 1, z$;	*(ii)* $y-1/2, -x + 1/2, -z + 3/2$;	

The coordination anion in compound **4**, shown in Figure 5, is a polymeric chain, parallel to the ***c*** axis, where $Cu_2(Ac)_4$ units with a paddle-wheel structure are connected to each other through bridging chlorido ligand. The symmetry of the anion corresponds to a fourfold roto-inversion axis, where chloride ligands lie on special positions with a Wyckoff label *c* (0, ½, ¼) and copper central atoms on special positions with a Wyckoff label *f* (0, ½, *z*). The Cu(II) central atoms also have a square-pyramidal coordination in this compound. The basal plane is formed by four O atoms of four bridging acetate ions at bond distances similar to those in compounds **1**–**3** (1.9647(15) and 1.9673(15) Å). The apical chlorido ligand is bonded at a slightly longer distance in comparison to those in compounds **1**–**3** (2.6726 (6) Å), since in compound **4**, this is a bridging ligand. Similar to compounds **1** and **3**, compound **4** also contains uncoordinated chloride anions and uncoordinated water molecules, while the charge is balanced in this compound by tetramethylammonium cations.

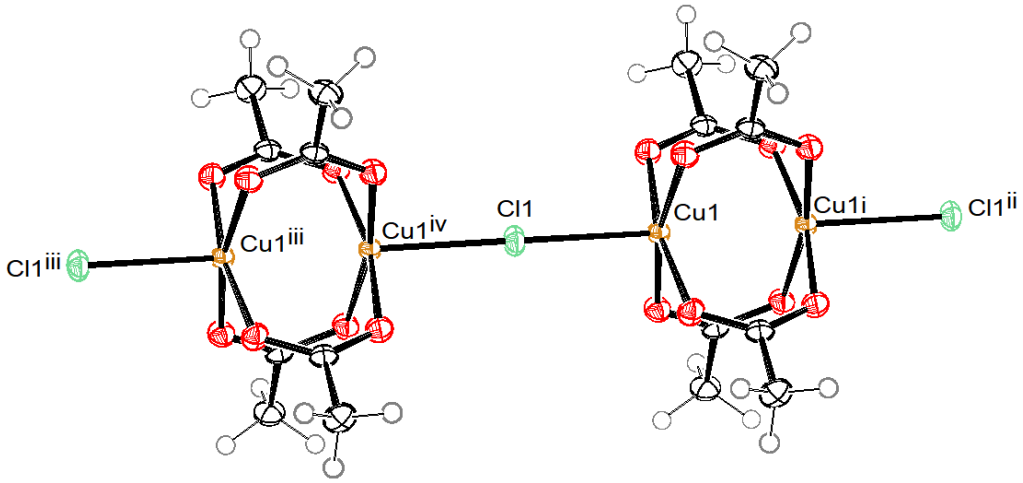


Figure 5. ORTEP drawing of a segment of the polymeric complex anion in compound **4** with labelling of Cu and Cl atoms. Ellipsoids are drawn at 50% level. (*i: y − 1/2, −x + 1/2, −z + 3/2; ii: x, y, z + 1; iii: x, y, z − 1; iv: y − 1/2, −x + 1/2, −z + 1/2*).

The crystal packing of compounds **1**–**4** is shown in Figures 6–9, respectively. It is stabilized by intermolecular hydrogen bonds, which are shown in these figures by cyan color. Their geometric parameters are given in Table 3. In compound **2**, dimethylammonium cations are hydrogen-bonded to dimeric coordination anions via N-H···Cl and via N-H···O intermolecular hydrogen bonds (N1-H···O1, N1-H···O3 and N1-H···$Cl1^{sr}$; sr stands for symmetry relation, given in Table 3. Compounds **1** and **3** also both contain uncoordinated water molecules. Each water molecule is a donor of two O-H···Cl hydrogen bonds to uncoordinated chloride anions (O1-H···Cl2 and O1-H···$Cl2^{sr}$). In both compounds, each water molecule is also an acceptor of one N-H···O hydrogen bond (N2-H···O1w and N1_H···O1w in **1** and **3**, respectively). Each cation is also hydrogen bonded to a dimeric complex anion via a N-H···Cl hydrogen bond (N1-H···$Cl1^{sr}$ and N2-H···$Cl1^{sr}$) and also in compound **3** via a N-H···O hydrogen bond (N2-H···O2). In compound **1**, there are N-H···O hydrogen bonds between cations and anions only between cations which are not hydrogen-bonded to water molecules. In compound **4**, tetramethylammonium cations do not have H atoms bonded to N atoms, and consequently, there are only hydrogen bonds, donated by water molecules. Each water molecule is a donor of an O-H···O hydrogen bond to another symmetrically related water molecule and to the uncoordinated chloride anion (O1w-H···Cl2 and O1w-H···$O1w^{sr}$), although in this compound, polymeric anions are not acceptors of classical hydrogen bonds. They are surrounded by a mantle consisting of tetramethylammonium cations, as shown in Figure 9.

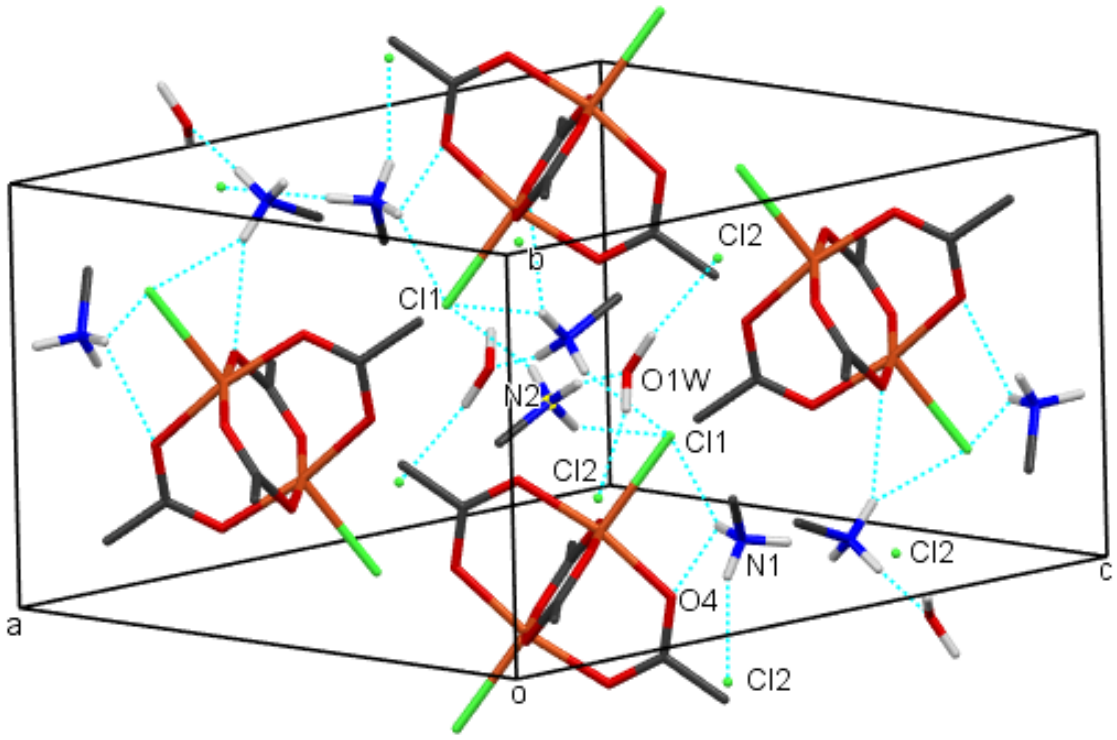


Figure 6. The packing of molecules of compound **1**, showing hydrogen bonds (cyan). H atoms from methyl groups were omitted for clarity. Color scheme: Cl (green), Cu (orange), C (gray), H (white), N (blue), O (red).

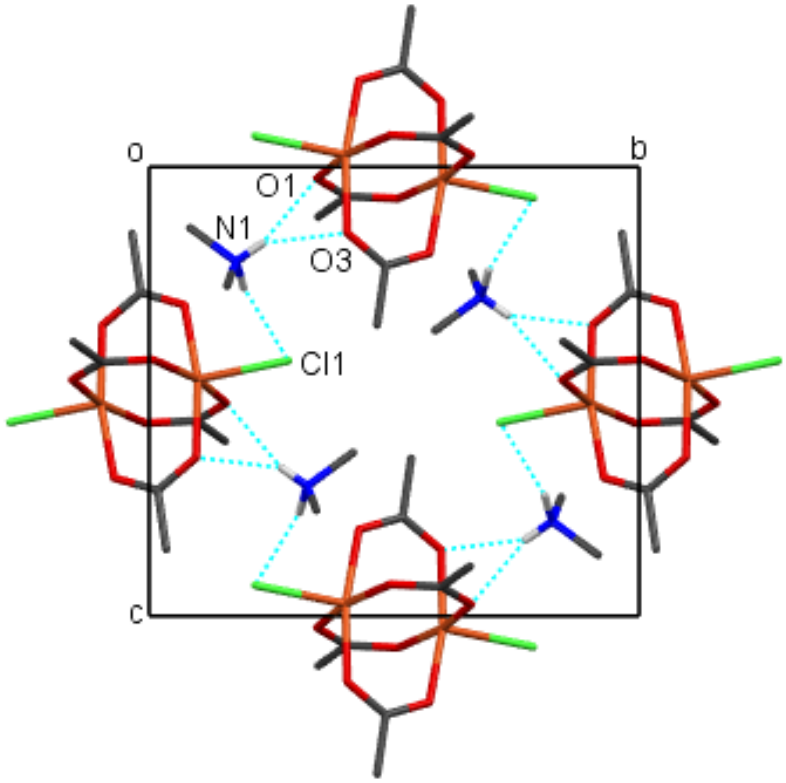


Figure 7. The packing of molecules of compound **2** viewed along the *a* axis, showing hydrogen bonds (cyan). H atoms from methyl groups were omitted for clarity. Color scheme: Cl (green), Cu (orange), C (gray), H (white), N (blue), O (red).

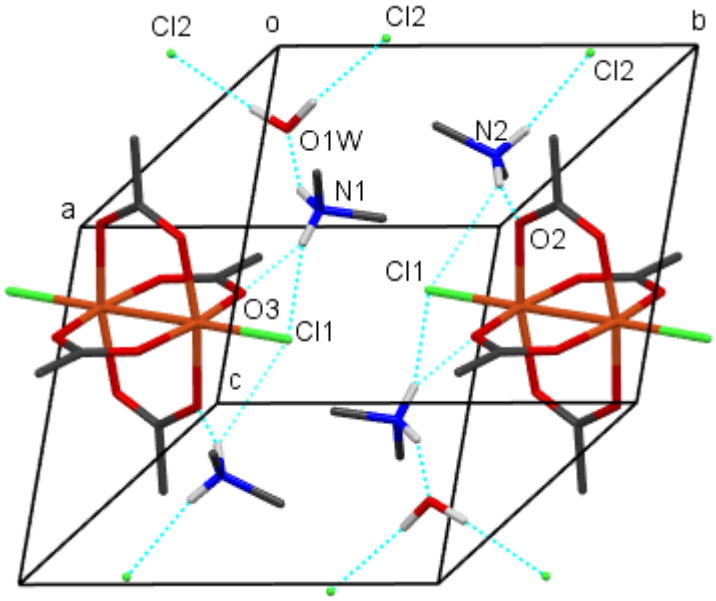


Figure 8. The packing of molecules of compound **3**, showing hydrogen bonds (cyan). H atoms from methyl groups were omitted for clarity. Color scheme: Cl (green), Cu (orange), C (gray), H (white), N (blue), O (red).

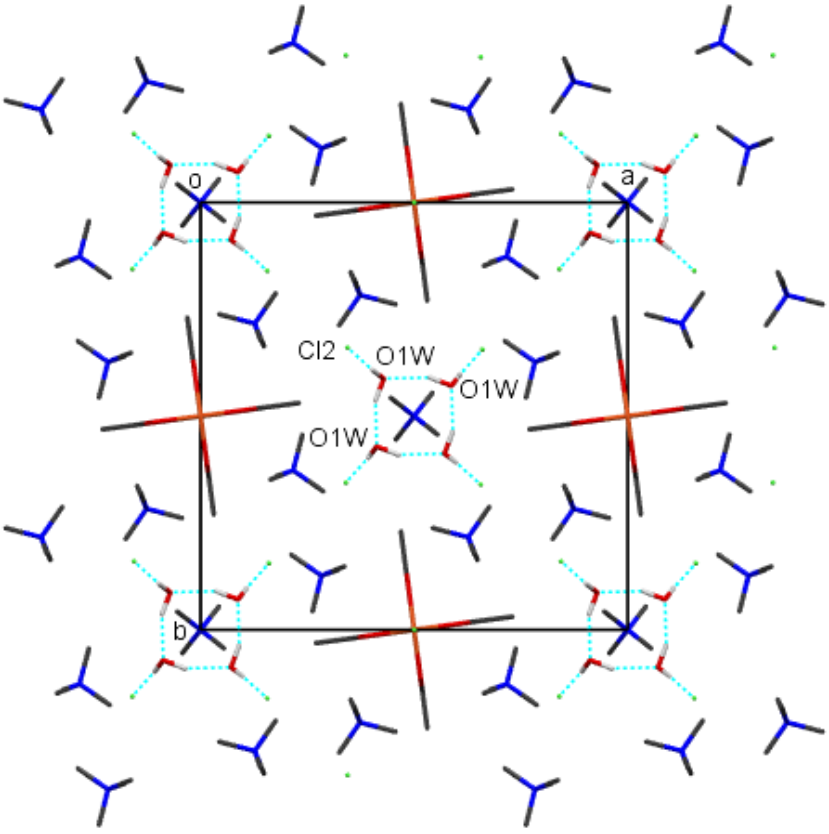


Figure 9. The packing of molecules of compound **4** viewed along the ***c*** axis, showing hydrogen bonds (cyan). H atoms from methyl groups were omitted for clarity. Color scheme: Cl (green), Cu (orange), C (gray), H (white), N (blue), O (red).

Table 3. Hydrogen bond geometry for **1–4**.

D-H···A	*d*(D-H) [Å]	*d*(H···A) [Å]	*d*(D···A) [Å]	<(DHA) [°]
1				
O1w-H2w1···Cl2^{i}	0.94(1)	2.23(1)	3.161(2)	173(3)
O1w-H1w1···Cl2	0.93(1)	2.27(1)	3.179(2)	166(2)
N1-H11···Cl2	0.94(3)	2.24(3)	3.166(2)	168(2)
N1-H12···Cl2	0.83(3)	2.41(3)	3.172(2)	154(2)
N1-H13···O4	0.90(3)	2.46(3)	3.090(2)	127(2)
N1-H13···Cl1^{ii}	0.90(3)	2.39(3)	3.186(2)	147(2)
N2-H21···O1w	0.91(3)	1.86(3)	2.739(3)	162(2)
N2-H22···Cl1^{iii}	0.91(3)	2.57(3)	3.381(2)	149(3)
N2-H23···Cl1^{iv}	0.87(3)	2.38(3)	3.195(2)	157(2)
(i) $2-x, -1/2+y, 3/2-z$;	*(ii)* $1-x, -y, 1-z$;	*(iii)* $1+x, 1/2-y, 1/2+z$	*(iv)* $2-x, -y, 1-z$	
2				
N1-H1···O1	0.79(3)	2.28(3)	2.962(3)	145(2)
N1-H1···O3	0.79(3)	2.45(3)	3.120(3)	144(2)
N1-H2···Cl1^{i}	0.90(3)	2.29(3)	3.140(2)	159(2)
(i) $1/2+x, 1/2-y, 1/2+z$				
3				
O1w-H2w1···Cl2^{i}	0.86(4)	2.34(4)	3.207(2)	176(3)
O1w-H1w1···Cl2	0.87(4)	2.31(4)	3.179(2)	174(3)
N1-H11···O1w	0.81(3)	2.06(3)	2.816(3)	156(2)
N1-H12···Cl1	0.83(3)	2.38(3)	3.162(2)	157(3)
N1-H12···O3	0.83(3)	2.59(3)	3.066(2)	118(2)
N2-H21···Cl2	0.86(3)	2.24(3)	3.098(2)	169(2)
N2-H22...O2	0.83(3)	2.20(3)	2.973(2)	154(2)
N2-H22···Cl1^{ii}	0.83(3)	2.80(3)	3.325(2)	123(2)
(i) $-x, -y, -z$; *(ii)* $1-x, -y, 1-z$				
4				
O1w-H2w1···Cl2	0.97(1)	2.09(1)	3.055(2)	175(3)
O1w-H1w1···O1w^{i}	0.95(1)	1.88(2)	2.780(3)	158(3)
(i) $y, 1-x, 1-z$				

The Cu···Cu separation between the two acetate-bridged Cu(II) centers is in dinuclear coordination compounds **1–3** in the interval of 2.4569(6) and 2.4626(6) Å. Other Cu atoms from neighboring anions are more than 7 Å away, with the shortest distances of 7.038(5), 7.163(5), and 7.187(6) Å in **1**, **2**, and **3**, respectively. In the polymeric coordination compound **4**, the Cu···Cu separation between the two acetate-bridged Cu(II) centers is slightly larger (2.6726(6) Å) in comparison to **1–3**. On the other hand, the Cu···Cu distance between neighboring dimeric units within the polymeric chain is significantly shorter than 7 Å (5.129(6) Å).

3.2. Thermal Analysis

The results of the thermogravimetric measurements of compounds **1–4** are presented in Figure 10. Compound **1** is thermally stable up to approximately 80 °C and decomposes in two distinguishable steps: the first one between 80 °C and 300 °C with a mass loss of 66% consists of three overlapping processes with peak temperatures at 140 °C, 190 °C, and 275 °C; and a second step between 350 °C and 700 °C with a mass loss of 14%. The observed total mass loss of approximately 80% between RT and 900 °C is in good agreement with the calculated mass loss for the decomposition of **1** to elemental copper (Δm_{calc} = 81%). Compound **2** features comparable thermal behavior, with the decomposition starting at a slightly higher temperature of 110 °C and proceeding in two major steps, the first one (consisting of two overlapping sub-steps with peak temperatures at 183 °C and 255 °C) between 110 °C and 270 °C (Δm_{obs} = 58%) and the second one between 340 °C and 750 °C (Δm_{obs} = 31%). Compound **3** decomposes in three partially overlapping steps, starting almost at RT and achieving a constant mass at 730 °C, with peak temperatures of 152 °C, 308 °C, and 630 °C. The overall observed mass loss between RT and 900 °C is 88.3%.

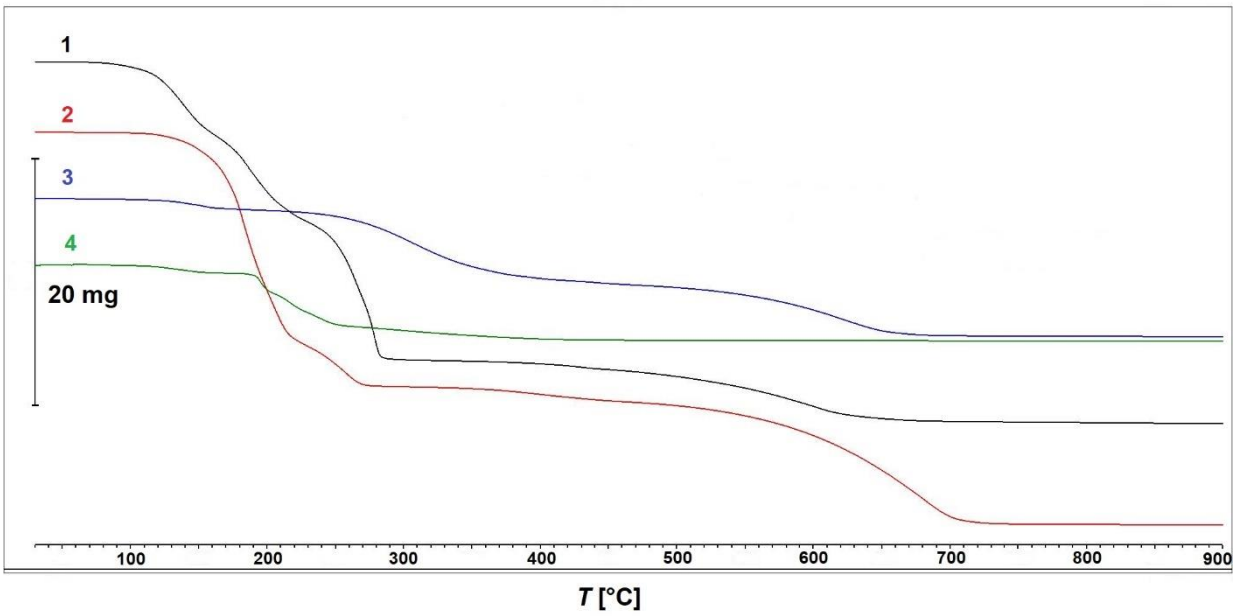


Figure 10. Thermogravimetric curves for compounds **1**–**4**.

Finally, complex **4** features a significantly different TGA curve when compared to (**1**–**3**). A small apparent mass gain at approximately 60 °C appears to be a measuring error. The compound decomposes over several overlapping steps between 110 °C and 450 °C, with the highest decomposition rate at approximately 195 °C. The decomposition of **4** is nearly finished at 480 °C, with the final decomposition step between approximately 550 °C and 700 °C, observed for (**1**–**3**), completely missing in **4**. Detailed thermogravimetric curves of all four compounds, including first derivative curves and mass losses, are provided as Supplementary Materials (Figures S1–S4). All residues obtained after thermal decomposition of (**1**–**4**) could be identified by powder X-ray diffraction as elemental copper, JCPDS No. 00-004-0836.

3.3. IR Spectra

The values of the N–H stretching vibrations have been observed in the area between 3500 and 3300 cm^{-1} [44] and compared for compounds **1**–**3**. For the determination of the asymmetric (ν_{as}) and symmetric (ν_s) vibrations of N–H stretching, the equation $\nu_s \approx 345.53 + 0.876 \cdot \nu_{as}$ can be used. In the area around 3400 cm^{-1}, the O–H stretching vibration of intra- and intermolecular hydrogen bonds is possible. There are also some vibrations around 3000 cm^{-1} (assigned to C–H stretching) and 2700 cm^{-1} (O–H stretching). Between 1650 and 1600 cm^{-1}, N–H deformations can be observed. The characteristic absorption bands for all four compounds are summarized in Table 4.

For carboxylate groups, the difference between the asymmetric and symmetric carboxylate stretches ($\Delta = \nu_{as}(COO^-) - \nu_s(COO^-)$) is often used to distinguish between monodentate, ionic, bridging or chelating carboxylate groups [45,46]:

Δ(monodentate) > Δ(ionic) > Δ(bridging bidentate) > Δ(chelating bidentate)

Since in compounds **1**–**4** there are chelate bidentate carboxylate groups, we can compare the values expected by the theory. The calculated Δ values for compound **1** are 141 and 140 cm^{-1}, which are larger than the values expected by the theory described above for chelating bidentate carboxylate groups. Similar values are also calculated for the other compounds (**2**: 106 and 120 cm^{-1}; **3**: 149 and 149 cm^{-1}; **4**: 153 and 150 cm^{-1}). The reason for such values could be strong intra- and intermolecular hydrogen bonds in/between the units of the compounds.

In the region around 1200 and 1000 cm^{-1}, C–N stretching frequencies are observed. At around 960 cm^{-1}, chlorates' stretching bands can be observed. In our compounds, these

values are slightly different due to the hydrogen bonds. The NH_3 rocking frequencies occur near 800 cm^{-1}, while around 680 cm^{-1}, O–H bending can be observed.

Table 4. Characteristic absorption bands in the IR spectra of the title compounds.

Compound				**Assignment**
1, cm^{-1}	**2**, cm^{-1}	**3**, cm^{-1}	**4**, cm^{-1}	
3443s, 3339s	3437m, 3375m	3444m, 3360m		ν_{as}(N–H) stretching ν_s(N–H) stretching
3037s, 3000s	3073m, 3020m	3010m, 2973m	3011m, 2943m	ν(C–H) stretching
1616s	1615s	1613s		ν(N–H) deformation
1603s, 1575s 1462s, 1435s	1569s, 1540s 1463s, 1420s	1594s, 1565s 1445s, 1416s	1592s, 1568s 1439s, 1418s	$\nu_{as}(COO^-)$ $\nu_s(COO^-)$
155m, 1030m	1053m, 1018s	1060s, 1019s	1049m, 1033s	ν(C–N) stretching
956s, 940s	940m	938m	955m	chlorates
848m	830m	837m		ν(N–H) rocking
682s	681s	678s	685s	ν(O–H) bending

3.4. Magnetic Properties

As shown in Figure 11, the $\chi(T)$ curves display a broad maximum between 240 K and 270 K, indicative of strong antiferromagnetic interactions between Cu(II) ions. This maximum reflects the energy scale of the exchange interaction, which is comparable to this temperature range. Upon further cooling, the susceptibilities decrease steadily, reaching a minimum between 100 K and 50 K. Below these temperatures, there is a steep increase, potentially pointing to the presence of paramagnetic impurities (e.g., uncoupled Cu(II) ions) or weak ferromagnetic contributions. The room temperature effective magnetic moments, calculated as $\mu_{eff} = \sqrt{8\chi T}$, range from 1.94 μ_B to 2.21 μ_B, exceeding the spin-only value for Cu(II) ions ($\mu_{eff} = 1.73\ \mu_B$) [47]. This suggests significant orbital contributions to the magnetic moment.

The antiferromagnetic interactions in copper dimers were modeled using the Bleaney–Bowers equation:

$$\chi = \frac{2N_A\mu_B g^2}{k_B T\left[3 + \exp\left(-\frac{2J}{k_B T}\right)\right]}(1-\rho) + \frac{N_A\mu_B g^2}{2k_B T}\rho,$$

where N_A is Avogadro's number, μ_B is the Bohr magneton, k_B is the Boltzmann constant, g is the Landé g-factor, J is the exchange constant, and ρ represents the molar ratio of uncoupled Cu(II) ions. The fitting of the susceptibility data to the Bleaney–Bowers model, performed between 30 K and room temperature, yielded the parameters summarized in Table 5. The best-fit lines are shown in the inset in Figure 11 as black lines.

Table 5. Fitting parameters g, J, and ρ obtained from the Bleaney–Bowers model for compounds **1**–**4**.

	Compound 1	**Compound 2**	**Compound 3**	**Compound 4**
g	2.21	2.30	2.14	2.34
J	–221 K	–215 K	–239 K	–217 K
ρ	5.4%	4.0%	8.2%	1.0%

The negative exchange constants J ranging from −215 K to −239 K confirm strong antiferromagnetic interactions between the Cu(II) ions. The small fraction of uncoupled ions, ranging from 1.0% to 8.2%, indicates that most of the Cu(II) ions are antiferromagnetically

coupled. The *g*-factors, which range from 2.14 to 2.34, are higher than the expected spin-only value of 2.00, suggesting significant orbital contributions due to spin–orbit coupling.

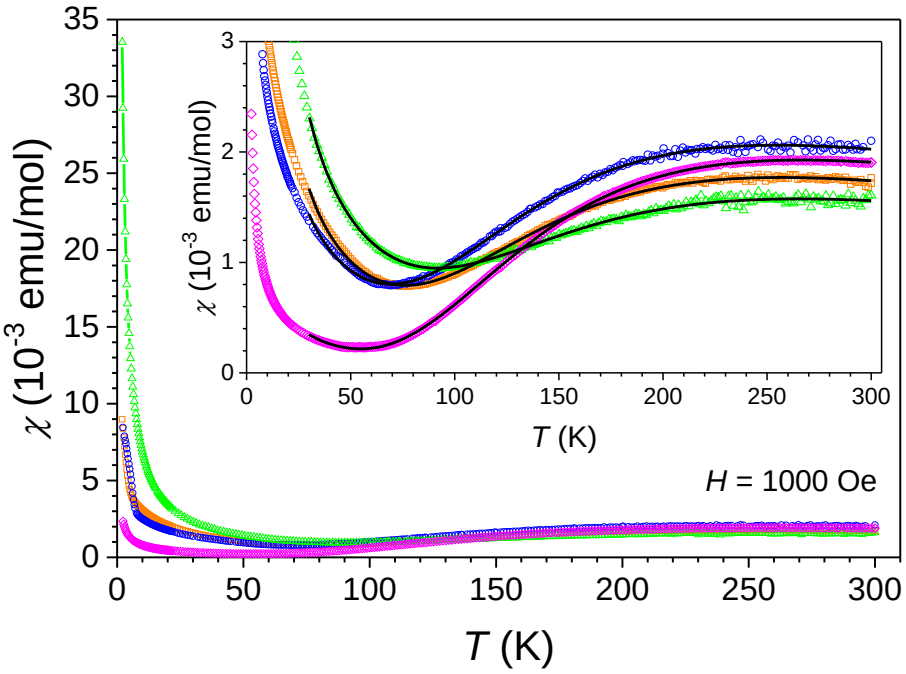


Figure 11. Temperature dependence of the magnetic susceptibility $\chi(T)$ of compounds **1** (orange squares), **2** (blue circles), **3** (green triangles), and **4** (purple diamond), measured in a DC magnetic field of 1000 Oe. The inset shows the zoomed-in susceptibility data for all compounds with corresponding Bleaney–Bowers best-fit lines (black lines).

To justify the use of the Bleaney–Bowers model for the chain-like compound **4**, an additional fitting with an alternating Cu(II) chain model was performed using the PHI software, version v3.1.6. [48]. The negligible value of J associated with the longer Cu-Cu distance ($J = 0.3$ K), compared to the shorter Cu-Cu distance ($J = -213$ K) in the chain, strongly supports the isolated dimer approach. For structurally similar binuclear Cu(II) complexes with bridging acetate and chloride ligands, the typical values for the coupling constant and the g-factor are around -240 K and (2.1–2.2), respectively [49–52], which are in good agreement with our values.

4. Conclusions

In this work, four copper-based coordination compounds with acetate and chlorine ligands and different methylammonium, dimethylammonium, and tetraethylammonium cations were successfully synthesized. The data obtained from single-crystal X-ray crystallography indicate that compounds **1**–**3** consist of a centrosymmetric dinuclear $[Cu_2(Ac)_4Cl_2]^{2-}$ anion with acetate ligands arranged in a *paddle-wheel* conformation. On the other hand, the coordination anion in compound **4** is a polymeric chain, with $Cu_2(Ac)_4$ units connected via bridging chloride ligands. The crystal packing of all compounds is stabilized by a rich network of N–H···O, N–H···Cl, and O–H···Cl hydrogen bonds. The Cu···Cu distances in dinuclear compounds **1**–**3** lie in the interval between 2.4569(6) and 2.4626(6) Å, whereas the Cu···Cu separation in the polymeric compound **4** is slightly larger (2.6726(6) Å).

Experimental data obtained from thermal and magnetic measurements are in good agreement with those obtained from structural investigations. Deviations of band positions between ideal values and those obtained in the IR spectra measured for **1**–**4** indicate the presence of strong hydrogen bonds in the structure. The results of the thermogravimetric analysis reveal a significantly different thermal behavior of the polymeric compound **4**

when compared to dimeric complexes **1–3**, while magnetic measurements indicate strong antiferromagnetic interactions between Cu(II) ions and significant orbital contributions to the magnetic moment.

Continuing studies of further coordination compounds of Cu(II) with halogenide and acetate ligands and different methylammonium-based cations, including trimethylammonium, as well as investigations of additional properties of those compounds, are underway.

Supplementary Materials: The following supporting information can be downloaded at: https://www.mdpi.com/article/10.3390/inorganics12100261/s1, Figures S1–S4: Detailed thermogravimetric curves of compounds **1–4**, including first derivative curves and mass losses; cif and checkcif files of compouds **1–4**.

Author Contributions: Conceptualization, M.K. and A.G.; Methodology, A.G., B.D., M.J. and M.K.; Investigation, A.G., B.D., M.J., A.S., A.P. and M.K.; Writing—Original Draft Preparation: A.G., A.S. and M.K.; Writing—Review and Editing: A.G., M.J. and M.K. All authors have read and agreed to the published version of the manuscript.

Funding: The authors acknowledge the support of the Centre for Research Infrastructure at the University of Ljubljana, Faculty of Chemistry and Chemical Technology, which is part of the Network of Research and Infrastructural Centres UL (MRIC UL) and is financially supported by the Slovenian Research Agency (Infrastructure programme No. I0-0022). M.J. acknowledges the financial support of the Slovenian Research Agency (Grant No. P2-0348). The financial support from the grant numbers P2-0006, P1-0175, and P1-0403 of the Slovenian Research Agency (ARRS) is also gratefully acknowledged.

Data Availability Statement: The original contributions presented in the study are included in the article, further inquiries can be directed to the corresponding author.

Conflicts of Interest: The authors declare no conflict of interest.

References

1. Mączka, M.; Ptak, M.; Gągor, A.; Stefańska, D.; Zaręba, J.K.; Sieradzki, A. Methylhydrazinium Lead Bromide: Noncentrosymmetric Three-Dimensional Perovskite with Exceptionally Large Framework Distortion and Green Photoluminescence. *Chem. Mater.* **2020**, *32*, 1667–1673. [CrossRef]
2. Fabini, D.H.; Labram, J.G.; Lehner, A.J.; Bechtel, J.S.; Evans, H.A.; Van der Ven, A.; Wudl, F.; Chabinyc, M.L.; Seshadri, R. Main-Group Halide Semiconductors Derived from Perovskite: Distinguishing Chemical, Structural, and Electronic Aspects. *Inorg. Chem.* **2017**, *56*, 11–25. [CrossRef] [PubMed]
3. Dionigi, C.; Goudjil, M.; Ruani, G.; Bindi, L. The Effect of Short Chain Carboxylic Acids as Additives on the Crystallization of Methylammonium Lead Triiodide (MAPI). *Inorganics* **2022**, *10*, 201. [CrossRef]
4. Oku, T.; Uchiya, S.; Okumura, R.; Suzuki, A.; Ono, I.; Fukunishi, S.; Tachikawa, T.; Hasegawa, T. Effects of Co-Addition of Guanidinium and Cesium to $CH_3NH_3PbI_3$ Perovskite Solar Cells. *Inorganics* **2023**, *11*, 273. [CrossRef]
5. Kubicki, D.J.; Prochowicz, D.; Salager, E.; Rakhmatullin, A.; Grey, C.P.; Emsley, L.; Stranks, S.D. Local Structure and Dynamics in Methylammonium, Formamidinium, and Cesium Tin(II) Mixed-Halide Perovskites from ^{119}Sn Solid-State NMR. *J. Am. Chem. Soc.* **2020**, *142*, 7813–7826. [CrossRef]
6. Gray, M.B.; Holzapfel, N.P.; Liu, T.; Da Cruz Pinha Barbosa, V.; Harvey, N.P.; Woodward, P.M. Synthesis, crystal chemistry, and optical properties of two methylammonium silver halides: $CH_3NH_3AgBr_2$ and $CH_3NH_3Ag_2I_3$. *J. Mater. Chem. C* **2021**, *9*, 9251–9259. [CrossRef]
7. Murasugi, H.; Kumagai, S.; Iguchi, H.; Yamashita, M.; Takaishi, S. Organic–Inorganic Hybrid Gold Halide Perovskites: Structural Diversity through Cation Size. *Chem. Eur. J.* **2019**, *25*, 9885–9891. [CrossRef]
8. Boča, M.; Svoboda, I.; Renz, F.; Fuess, H. Poly[methylammonium tris(μ_2-formato-κ^2O:O′)cobalt(II)]. *Acta Crystallogr. C* **2004**, *60*, m631–m633. [CrossRef]
9. Gerasimenko, A.V.; Davidovich, R.L.; Logvinova, V.B. Crystal structures of layered zirconium pentafluorides of methylammonium, glycinium, and β-alanine. *J. Struct. Chem.* **2011**, *52*, 524–530. [CrossRef]
10. Bujak, M.; Angel, R.J. Single crystal X-ray diffraction studies on $[(CH_3)_nNH_{4-n}]_3[Sb_2Cl_9]$ (n = 2, 3) chloroantimonates(III) in their low-temperature ferroelectric phases—Structures and phase transitions. *J. Solid State Chem.* **2005**, *178*, 2237–2246. [CrossRef]
11. Conry, R.R. Copper: Inorganic & Coordination Chemistry. Based in part on the article Copper: Inorganic & Coordination Chemistry by Rebecca R. Conry & Kenneth D. Karlin which appeared in the *Encyclopedia of Inorganic Chemistry, First Edition*. In *Encyclopedia of Inorganic and Bioinorganic Chemistry*; Scott, R.A., Ed.; Wiley: Hoboken, NJ, USA, 2011. [CrossRef]
12. Steinhauser, G.; Karaghiosoff, K.; Klapötke, T.M. Synthesis and Crystal Structure of $(CH_3NH_3)_2[Cu(NO_3)_4]$: A Rare Example of a Tetranitratocuprate(II) with a Light Cation of the Type $M_2[Cu(NO_3)_4]$. *Z. Anorg. Allg. Chem.* **2008**, *634*, 892–894. [CrossRef]

13. Afonin, E.G.; Aleksandrov, G.G.; Sergienko, V.S. Synthesis and properties of protonated methylammonium bis(1-hydroxyethane-1,1-diphosphonato)cuprates(II).: Crystal structure of $(CH_3NH_3)_2[Cu(H_2O)(H_2L)_2]\cdot H_2O$. *Russ. J. Coord. Chem.* **1999**, *25*, 863–869.
14. Martin, J.D.; Yang, J.; Dattelbaum, A.M. Templated Synthesis of Cuprous Chloride Networks: Synthesis and Characterization of $[Hpy]Cu_3Cl_6$ and $\{[H_3NMe]Cl\}[H_3NMe]_2Cu_9Cl_{16}$. *Chem. Mater.* **2001**, *13*, 392–399. [CrossRef]
15. Groeneveld, B.G.H.M.; Duim, H.; Kahmann, S.; De Luca, O.; Tekelenburg, E.K.; Kamminga, M.E.; Protesescu, L.; Portale, G.; Blake, G.R.; Rudolf, P.; et al. Photochromism in Ruddlesden–Popper copper-based perovskites: A light-induced change of coordination number at the surface. *J. Mater. Chem. C* **2020**, *8*, 15377. [CrossRef]
16. Lu, J.-L.; Zhang, D.-S.; Li, L.; Liu, B.P. Bis(dimethylammonium) bis(pyridine-2,5-dicarboxylato)copper(II). *Acta Crystallogr. E* **2006**, *62*, m3321–m3322. [CrossRef]
17. Demir, S.; Çepni, H.M.; Hołyńska, M.; Kavanoz, M. A tetranuclear copper (II) complex with pyrazole-3,5-dicarboxylate ligands: Synthesis, characterization and electrochemical properties. *Z. Naturforsch. B* **2016**, *71*, 305–310. [CrossRef]
18. Burrows, A.D.; Mahon, M.F.; Sebestyen, V.M.; Lan, Y.; Powell, A.K. Synthesis, Structures, And Magnetic Behavior of New Anionic Copper(II) Sulfate Aggregates and Chains. *Inorg. Chem.* **2012**, *51*, 10983–10989. [CrossRef]
19. Stone, M.B.; Tian, W.; Granroth, G.E.; Lumdsen, M.D.; Chung, J.-H.; Mandrus, D.G.; Nagler, S.E. Spin dynamics of the low-dimensional magnet $(CH_3)_2NH_2CuCl_3$. *Physica B* **2006**, *385–386*, 438–440. [CrossRef]
20. Kirpichnikova, L.F.; Pietraszko, A.; Bednarski, W.; Waplak, S.; Sheleg, A.U. Crystal Structure and Phase Transitions in the New Crystals of $[(CH_3)_2NH_2]_2CuCl_4[(CH_3)_2NH_2]Cl$. *Crystallogr. Rep.* **2004**, *49*, 92–100. [CrossRef]
21. Awwadi, F.; Willett, R.D.; Twamley, B.; Shneider, R.; Landee, C.P. Strong Rail Spin $^1/_2$ Antiferromagnetic Ladder Systems: (Dimethylammonium)(3,5-Dimethylpyridinium)CuX_4, X = Cl, Br. *Inorg. Chem.* **2008**, *47*, 9327–9332. [CrossRef]
22. Salimi, S.; Akhbari, K.; Farhia, S.M.F.; White, J.M. Sonochemical synthesis and crystal structure of copper(II)-based biodegradable antibacterial scaffold. *J. Mol. Struct.* **2022**, *1267*, 133521. [CrossRef]
23. Gupta, K.; Biswas, B.; Mallick, S.; Rizzoli, C.; Saha, S.K.; Roy, U.K.; Saha, R. Insight on the presence of dimethylammonium cation within anionic metal-organic supramolecular host: Structural, Hirshfeld surface, optical and theoretical analysis. *J. Coord. Chem.* **2023**, *76*, 1553–1566. [CrossRef]
24. Powell, R.E.; Lees, M.R.; Tizzard, G.J.; Coles, S.J.; Yuan, Q.; Van Koningsbruggen, P.J. Fe^{III} in the high-spin state in dimethylammonium bis [3-ethoxysalicylaldehyde thiosemicarbazonato(2–)-κ^3O^2,N^1,S]ferrate(III). *Acta Crystallogr. C* **2023**, *79*, 18–24. [CrossRef] [PubMed]
25. Abdelhadi, A.B.; Rodriguez-Sánchez, S.; Ouarsal, R.; Saadi, M.; El Ammari, L.; Morley, N.; El Bali, B.; Gómez-Torres, Ó.; Lachkar, M.; Douhal, A. Synthesis, characterization, and magnetic and antibacterial properties of a novel iron(iii) complex $(CH_3)_2NH_2[Fe(phen)Cl_4]$. *Mater. Adv.* **2024**, *5*, 3058–3066. [CrossRef]
26. Peksa, P.; Nowok, A.; Formalik, F.; Zaręba, J.K.; Trzimiel, J.; Gągor, A.; Mączka, M.; Sieradzki, A. More complex than originally thought: Revisiting the origins of the relaxation processes in dimethylammonium zinc formate. *J. Mater. Chem. C* **2022**, *10*, 6866–6877. [CrossRef]
27. Sharif, S.; Saeed, M.; Dege, N.; Bano, R.; Gilani, M.A.; Şahin, O.; Ahmad, S.; Ch, A.R. Solvothermal synthesis, crystal structure, thermal, magnetic properties and DFT computations of a Ytterbium(III) complex derived from pyridine-2,6-dicarboxylic acid. *J. Mol. Struct.* **2022**, *1260*, 132877. [CrossRef]
28. Ivanova, A.A.; Gontcharenko, V.E.; Lunev, A.M.; Sidoruk, A.; Arkhipov, I.A.; Taydakov, I.V.; Belousov, Y.A. New Carboxylate Anionic Sm-MOF: Synthesis, Structure and Effect of the Isomorphic Substitution of Sm^{3+} with Gd^{3+} and Tb^{3+} Ions on the Luminescent Properties. *Inorganics* **2022**, *10*, 104. [CrossRef]
29. Mautner, F.A.; Hanna, S.; Cortés, R.; Lezama, L.; Gotzone Barandinka, M.; Rojo, T. Crystal Structure and Spectroscopic and Magnetic Properties of the Manganese(II) and Copper(II) Azido-Tetramethylammonium Systems. *Inorg. Chem.* **1999**, *38*, 4647–4652. [CrossRef]
30. Liu, X.; Guo, G.-C.; Wu, A.-Q.; Ci, L.-Z.; Huang, J.-S. Two Halogeno(cyano)cuprates with Long-Lived and Strong Luminescence. *Inorg. Chem.* **2005**, *44*, 4282–4286. [CrossRef]
31. Jalilian, E.; Lidin, S. Size matters-sometimes. The $[Cu_xI_y]^{(y-x)-}(NR_4)^+_{(y-x)}$ systems. *CrystEngComm* **2011**, *13*, 5730–5736. [CrossRef]
32. Vilela, R.S.; Oliveira, T.L.; Martins, F.T.; Ellena, J.A.; Lloret, F.; Julve, M.; Cangussu, D. Synthesis, crystal structure and magnetic properties of the helical oxalate-bridged copper(II) chain $\{[(CH_3)_4N]_2[Cu(C_2O_4)_2]\cdot H_2O\}_n$. *Comptes Rendus Chim.* **2012**, *15*, 856–865. [CrossRef]
33. Fernandes, T.S.; Vilela, R.S.; Valdo, A.K.; Martins, F.T.; García-España, E.; Inclán, M.; Cano, J.; Lloret, F.; Julve, M.; Stumpf, H.O.; et al. Dicopper(II) Metallacyclophanes with *N,N′*-2,6-Pyridinebis(oxamate): Solution Study, Synthesis, Crystal Structures, and Magnetic Properties. *Inorg. Chem.* **2016**, *55*, 2390–2401. [CrossRef]
34. Grancha, T.; Ferrando-Soria, J.; Armentano, D.; Pardo, E. Synthesis of a chiral rod-like metal–organic framework from a preformed amino acid-based hexanuclear wheel. *J. Coord. Chem.* **2019**, *72*, 1204–1221. [CrossRef]
35. Nicholas, A.D.; Bullard, R.M.; Wheaton, A.M.; Streep, M.; Nicholas, V.A.; Pike, R.D.; Patterson, H.H. Synthesis and Luminescence of Optical Memory Active Tetramethylammonium Cyanocuprate(I) 3D Networks. *Materials* **2019**, *12*, 1211. [CrossRef]
36. Hassan, N.; Nagaraja, S.; Saha, S.; Tarafder, K.; Ballav, N. Excitonic cuprophilic interactions in one-dimensional hybrid organic–inorganic crystals. *Chem. Sci.* **2024**, *15*, 4075–4085. [CrossRef] [PubMed]

37. Koziskova, J.; Hahn, F.; Richter, J.; Kožišek, J. Comparison of different absorption corrections on the model structure of tetrakis(μ_2-acetato)-diaqua-di-copper(II). *Acta Chim. Slovaca* **2016**, *9*, 136–140. [CrossRef]
38. Rigaku Oxford Diffraction. *CrysAlisPro*, Version 1.171.39.46e; Rigaku Oxford Diffraction: The Woodlands, TX, USA, 2018.
39. Altomare, A.; Burla, M.C.; Camalli, M.; Cascarano, G.L.; Giacovazzo, C.; Guagliardi, A.; Moliterni, A.G.G.; Polidori, G.; Spagna, R. *SIR*97: A new tool for crystal structure determination and refinement. *J. Appl. Crystallogr.* **1999**, *32*, 115–119. [CrossRef]
40. Sheldrick, G.M. Crystal structure refinement with *SHELXL*. *Acta Crystallogr. C* **2015**, *71*, 3–8. [CrossRef]
41. Farrugia, J.L. *ORTEP*-3 for Windows—A version of *ORTEP*-3 with a Graphical User Interface (GUI). *J. Appl. Crystallogr.* **1997**, *30*, 565. [CrossRef]
42. Macrae, C.F.; Edgington, P.R.; McCabe, P.; Pidcock, E.; Shields, G.P.; Taylor, R.; Towler, M.; Van de Streek, J. *Mercury*: Visualization and analysis of crystal structures. *J. Appl. Crystallogr.* **2006**, *39*, 453–457. [CrossRef]
43. Kahn, O. *Molecular Magnetism*; VCH Publishing: Weinheim, Germany; New York, NY, USA, 1993. [CrossRef]
44. Bellamy, L.J. *The Infrared Spectra of Complex Molecules*, 3rd ed.; Chapman and Hall: London, UK, 1975. [CrossRef]
45. Martini, D.; Pellei, M.; Pettinari, C.; Skelton, B.W.; White, A.H. Synthesis, spectroscopic and structural characterization of Cu(II) derivatives of tris(pyrazol-1-yl)methanes. *Inorganica Chim. Acta* **2002**, *333*, 72–82. [CrossRef]
46. Vargová, Z.; Zenlenák, V.; Cisarová, I.; Györyová, K. Correlation of thermal and spectral properties of zinc(II) complexes of pyridinecarboxylic acids with their crystal structures. *Thermochim. Acta* **2004**, *423*, 149–157. [CrossRef]
47. Ashcroft, N.W.; Mermin, N.D. *Solid State Physics*; Saunders College Publishing: Philadelphia, PA, USA, 1976.
48. Chilton, N.F.; Anderson, R.P.; Turner, L.D.; Soncini, A.; Murray, K.S. PHI: A powerful new program for the analysis of anisotropic monomeric and exchange-coupled polynuclear d- and f-block complexes. *J. Comput. Chem.* **2013**, *34*, 1164–1175. [CrossRef] [PubMed]
49. Mikuriya, M.; Yamakawa, C.; Tanabe, K.; Nukita, R.; Amabe, Y.; Yoshioka, D.; Mitsuhashi, R.; Tatehata, R.; Tanaka, H.; Handa, M.; et al. Copper(II) Carboxylates with 2,3,4-Trimethoxybenzoate and 2,4,6-Trimethoxybenzoate: Dinuclear Cu(II) Cluster and μ-Aqua-Bridged Cu(II) Chain Molecule. *Magnetochemistry* **2021**, *7*, 35. [CrossRef]
50. Kristl, M.; Šturm, J.; Golobič, A.; Jagličić, Z.; Dojer, B. New copper(II) complexes with hydroxypyridines: Synthesis, structural, thermal, and magnetic properties. *Inorganica Chim. Acta* **2023**, *556*, 121670. [CrossRef]
51. Kato, M.; Muto, Y. Factors affecting the magnetic properties of dimeric copper(II) complexes. *Coord. Chem. Rev.* **1988**, *92*, 45–83. [CrossRef]
52. Kozlevčar, B.; Gamez, P.; De Gelder, R.; Jagličić, Z.; Strauch, P.; Kitanovski, N.; Reedijk, J. Counterion and Solvent Effects on the Primary Coordination Sphere of Copper(II) Bis(3,5-dimethylpyrazol-1-yl)acetic Acid Coordination Compounds. *Eur. J. Inorg. Chem.* **2011**, *2011*, 3650–3655. [CrossRef]

Disclaimer/Publisher's Note: The statements, opinions and data contained in all publications are solely those of the individual author(s) and contributor(s) and not of MDPI and/or the editor(s). MDPI and/or the editor(s) disclaim responsibility for any injury to people or property resulting from any ideas, methods, instructions or products referred to in the content.